

UNIVERZITA KOMENSKÉHO V BRATISLAVE
FAKULTA MATEMATIKY, FYZIKY A INFORMATIKY



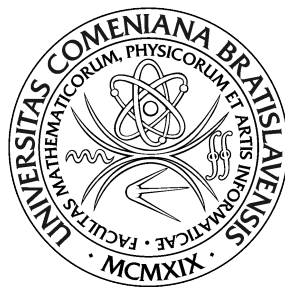
NA EFEKTÍVNE KONŠTRUOVANIE TRACKLETOV OBJEKTOV VE

Diplomová práca

2017

Bc. Stanislav Krajčovič

UNIVERZITA KOMENSKÉHO V BRATISLAVE
FAKULTA MATEMATIKY, FYZIKY A INFORMATIKY



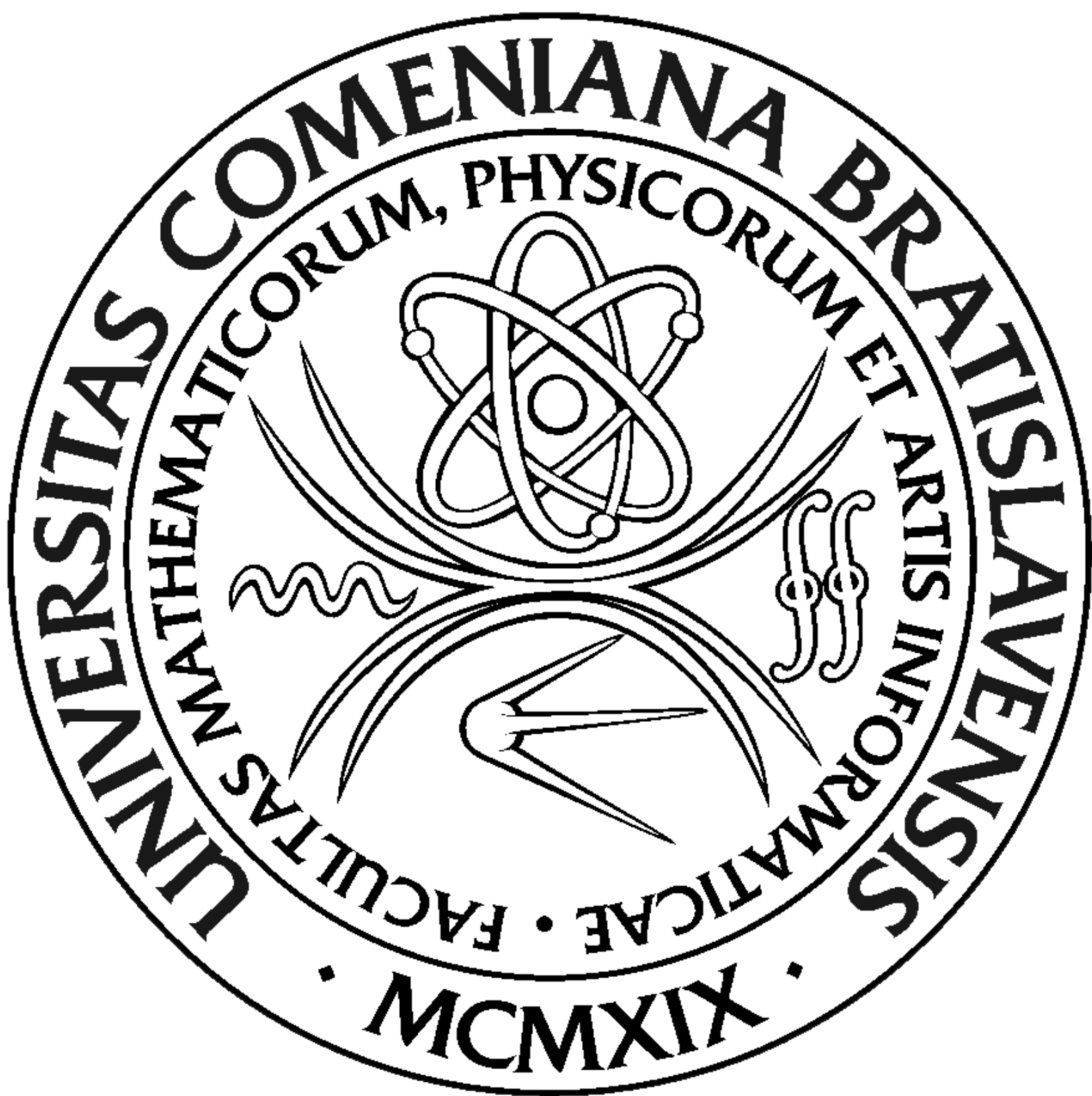
NA EFEKTÍVNE KONŠTRUOVANIE TRACKLETOV OBJEKTOV VE

Diplomová práca

Študijný program: Aplikovaná informatika
Študijný odbor: 2511 Aplikovaná informatika
Školiace pracovisko: Katedra aplikovanej informatiky
Školiteľ: prof. RNDr. Roman Ďurikovič, PhD.

Bratislava, 2017

Bc. Stanislav Krajčovič



Čestne prehlasujem, že túto diplomovú prácu som
vypracoval samostatne len s použitím uvedenej literatúry
a za pomoci konzultácií u môjho školiteľa.

Bratislava, 2017

.....

Bc. Stanislav Krajčovič

Pod'akovanie

Touto cestou by som sa chcel v prvom rade poďakovať môjmu školiteľovi prof. RNDr. Romanovi Ďurikovičovi, PhD. za jeho cenné rady a usmerenia, ktoré mi veľmi pomohli pri riešení tejto diplomovej práce. Takisto sa chcem poďakovať mojím kolegom z YACGS semináru za rady ohľadom implementácie a v neposlednom rade chcem tiež poďakovať všetkým mojím kamarátom a celej mojej rodine za podporu počas môjho štúdia.

Abstrakt

Počas astronomických pozorovaní sa získavajú snímky nočnej oblohy, prevažne jej konkrétnej časti, ktoré sa ukladajú do tzv. Flexible Image Transport System (FITS) formátu. Tieto snímky obsahujú signál rôzneho charakteru od šumu spôsobeného elektrickým prúdom a vyčítavaním snímky zo CCD kamier, cez pozadie oblohy až po skutočné objekty ako hviezdy alebo objekty slnečnej sústavy (asteroidy, kométy, vesmírny odpad, atď.). Každý pixel FITS snímky je charakteristický svojou pozíciou na CCD kamere (x,y) a intenzitou. Tieto údaje sa využívajú na výpočet polohy objektu na CCD snímke a na jeho súhrnú intenzitu. Na typických astronomických snímkach sa hviezdy javia ako statické body, ktoré možno popísať tzv. rozptýlovou funkciou (z ang. Point Spread Function). To neplatí v prípade, keď sa uskutočnia pozorovania vesmírneho odpadu, ktorý sa pohybuje relatívne rýchlo vzhľadom k hviezdному pozadiu. V tomto prípade sa objekty javia ako predĺžené čiary a nie ako body. Ak sa počas pozorovaní ďalekohľad pohybuje za objektom vesmírneho odpadu nastáva situácia, že všetky hviezdy sa javia ako predĺžené čiary s rovnakou dĺžkou a smerom, zatiaľ čo snímaný objekt sa javí ako bod. Úlohou študenta/-ky bude naštudovať si literatúru venujúcu sa spracovaniu astronomických FITS snímok, ktoré obsahujú objekty vesmírneho odpadu. Následne študent/-ka navrhne najvhodnejší, alebo aj vlastný algoritmus na segmentáciu snímok, ktorý následne naprogramuje

a otestuje. Počas segmentácie sa identifikujú všetky objekty na snímke a pre každý taký objekt sa vyextrahuje jeho pozícia na CCD snímke (x,y) ako aj súhrnná intenzita. Testovanie algoritmu bude uskutočnené na reálnych snímkach na ktorých sa nachádza hviezdne pozadie ako aj vesmírny odpad. Výsledky sa porovnajú s predpoveďami pozícií vesmírneho odpadu, ktoré budú študentovi dodané spolu s reálnymi snímkami získanými ďalekohľadmi na Astronomickom a geofyzikálnom observatóriu v Modre, FMFI UK.

Kľúčové slová: vesmírny odpad, pozorovanie

Abstract

Keywords: space debris, observation

Contents

1	Introduction	1
2	Introduction to space debris and observations	2
2.0.1	Small space debris	4
2.0.2	Large space debris	10
2.1	Observations and telescopes	13
2.1.1	ESA OGS	14
2.1.2	FMPI AGO	16
3	Object dynamics	18
3.1	Kepler’s laws of orbital motion	18
3.2	Equatorial coordinate system	18
3.3	CCD and image reference frame	18
3.4	Image processing, segmentation and astrometric reduction . .	18
3.5	Initial orbit determination problem	19
4	Existing solutions to the problem of tracklet building	20
4.1	kd-trees	20
4.1.1	Efficient intra- and inter-night linking of asteroid de- tections using kd-trees	20
4.2	Uniform linear motion detection	20

4.2.1	Optical observation, image-processing, and detection of space debris in GEO	20
5	Technical and practical requirements	21
5.1	Input data	21
5.1.1	Flexible Image Transport System files	22
5.1.2	.cat files	25
5.1.3	Processing server parameters	27
6	Proposed solutions	28
6.1	Use of linear regression	28
6.2	Use of neural network	28
6.3	Use of the Initial Orbit Determination algorithms	28
6.4	Use of Hough transform	28
7	Design and implementation	29
8	Results	30
8.1	TDM, MPC, and CCSDS data formats	30
8.2	Visualization of results	30
8.3	Parameters	30
9	Conclusion	31

Chapter 1

Introduction

"Space debris" is a term which encompasses both natural and artificial objects and particles. While man-made objects, or "orbit debris", typically orbit around the Earth, meteoroids orbit around the sun and can have trajectories crossing that of the Earth.

There are many risks accompanied by the existence of space debris, namely in-orbit collisions with operational spacecraft, and re-entries. Impacts by millimetre-sized debris could disable a subsystem of an operational spacecraft, debris larger than 1 centimetre would disable the whole spacecraft and debris larger than 10 centimetres would cause catastrophic break-ups. Due to this fact it is important to observe and catalogue debris to prevent collisions with functional man-made satellites and re-entries which could endanger populace.

The aim of this diploma thesis is to develop a comprehensive algorithm and analyse different possible approaches which would identify space debris and extract its position from astronomical CCD images containing observations of star background and unknown objects.

Chapter 2

Introduction to space debris and observations

The term space debris encompasses all artificial non-functional objects orbiting around Earth. Each object has different physical properties, such as size and shape and is made of different materials which determine its behaviour and ease of tracking. Usually, in literature, space debris is categorized into four different groups by its type:

1. mission-related debris,
2. fragmentation debris,
3. non-functional spacecraft,
4. rocket bodies.

Despite having many different sources and causes, the clearest line is drawn between debris released intentionally and unintentionally. Examples of the former are launch adapters, lens covers, and many other components associated with launch events and payload deployment. The latter category

CHAPTER 2. INTRODUCTION TO SPACE DEBRIS AND OBSERVATIONS3

contains protective gloves, cooling liquids, or small particles released from material decay. Common feature of all these objects is that it's referred to as mission-related debris as well because it's result of a spacecraft's deployment, activation or operation [Kli06].

The polar opposite of mission-related debris is fragmentation debris. As the name indicates, it's objects or particles created during destructive disassociation of a rocket body or an orbital payload and as a result of deterioration when smaller-than-the-parent-object fragments are created. Breakups may be intentional or accidental and are the largest portion of catalogued orbital debris. Products of breakups are ejected into the surrounding area in toroidal cloud with various initial velocities and spread until they reach the limit of maximum inclination and altitudes of the debris [otPUoOSSS99].

Another commonly mentioned type of space debris in various literature is non-functional spacecraft. First deployed man-made satellite was Sputnik-1 on October 4, 1957. As of January 2017, there have been 5253 launches of human-made objects into space since then [ESA17]. Even though not all of them were satellites, they still are a common source of breakup events and the following creation of orbital debris. However, a satellite doesn't have to break into smaller pieces to be considered debris. Functional spacecrafts that reach their end of life are either re-orbited or left in their former orbit. Historically, re-orbiting manoeuvres were performed only in GEO orbit and by spacecrafts carrying nuclear material in LEO orbit, as well as for vehicles with crew and for reconnaissance. Nevertheless, according to the Mitigation Guidelines released in 2002 by Inter-Agency Space Debris Coordination Committee (IADC), spacecrafts in LEO should be allowed to fall into the atmosphere and burn up within 25 years of mission end and spacecrafts in GEO should be re-orbited at least 300 kilometres above the GEO orbital

ring and left in so-called “graveyard orbit”. Satellites in GEO are not lowered because it’s not efficient to carry extra fuel specifically for this purpose.

The last category of orbital debris consists of rocket bodies. Spacecrafts which are placed into orbit for their missions are launched on vehicles which are constructed for this single purpose. Deployment process has one or more stages that are represented by rocket bodies. The number of rocket bodies needed for ascent into desired altitude is proportional to the altitude – for example spacecrafts with missions in LEO only need one rocket body while those in GEO need may need up to three. First stages need to have enough thrust to lift the satellite despite gravity and air resistance and are generally bigger than other stages which are used to position the spacecraft in the final steps of deployment. As such, larger rocket bodies usually re-enter into the atmosphere and burn up or fall into the ocean, while the smaller stages are left at various altitudes. This kind of space debris poses danger especially because of its large dimensions and potentially leftover fuel that may cause explosions.

2.0.1 Small space debris

The size of space debris varies from particles less than one millimetre small to objects more than one metre large. While the smallest particles are difficult to track, the amount of those that have size less than 1 centimetre is estimated to be more than 170 million [ESA17]. Other sources list the population of debris with diameters bigger than 1 mm as $3 \cdot 10^8$ objects and $3 \cdot 10^{13}$ objects with diameter bigger than 1 μm [Kli06].

A major source of sub-centimetre reproductive space debris is the effect of harsh space environment on spacecraft surface materials. Intense UV radiation and atomic oxygen cause decay on spacecraft surfaces which is usually

coated in paint for thermal purposes, or other thermal protection materials. Erosion is enhanced through transits through the Earth shadow, when the temperature shifts and the material expands and shrinks. Paint flakes, such as one in Figure 2.1, created by these processes have small initial velocity and in combination with their relatively small size are not as dangerous to functional satellites though they can cause significant damage. They are categorised as fragmentation or sometimes as anomalous debris.

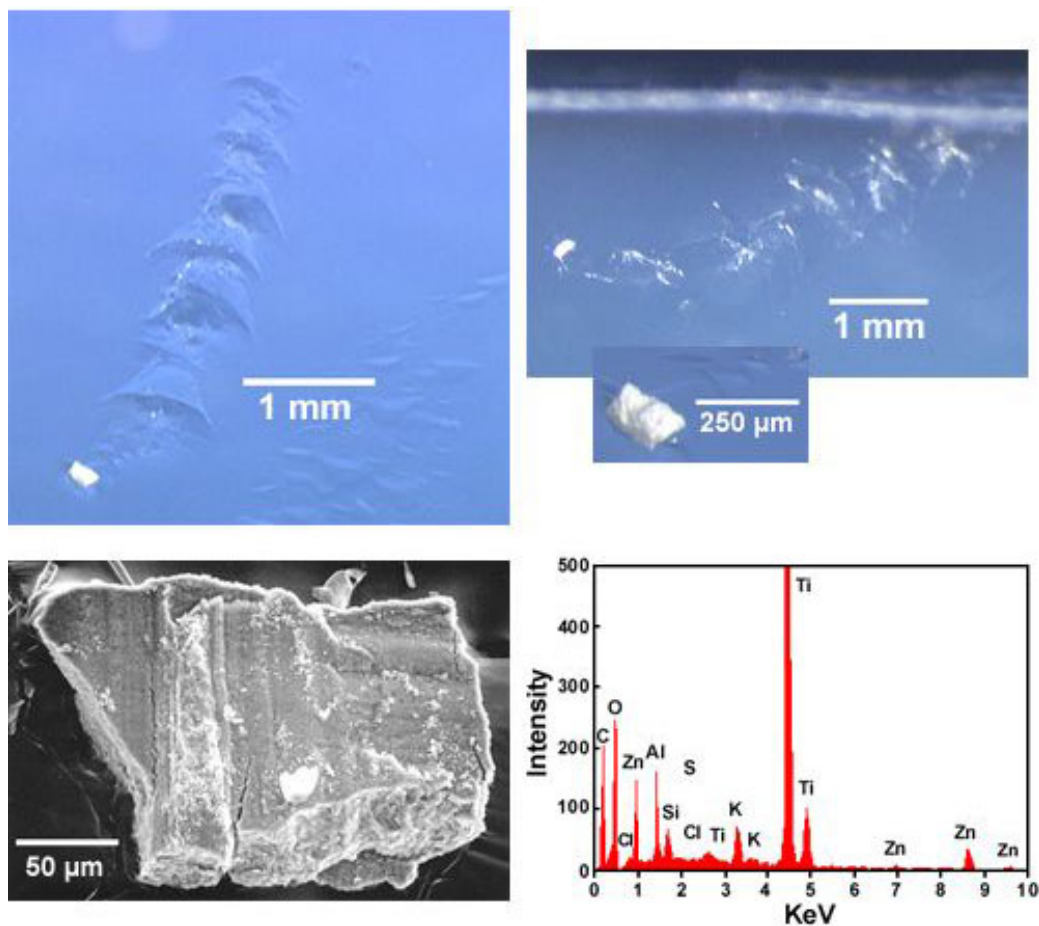


Figure 2.1: Paint flakes captured by Mir Environmental Effects Payload

Hypervelocity collisions of small debris objects create particles upon impact which are called ejecta and are part of the fragmentation debris group.

When assessing the number of small particles, it's important to acknowledge small meteoroids as well. This type of debris is not detectable from ground and is measured by examining surfaces of spacecrafts returned to Earth or by dedicated debris detectors situated in LEO altitudes. The most successful method for this is chemical analysis of impact craters. However, because of the mentioned high speeds of many of these particles, the pressure under which the impact is made is more than 100 GPa and temperatures more than 9000 degrees Celsius [Kli06]. As a result of this there is only a little impacting material left on the surface since most of it evaporates. Another important attribute which can be deduced from impact craters, though not easily, is size of the impactor. On the other hand, time and position of spacecraft in orbit is almost impossible to determine from impact craters. Figure 2.2 shows a hypervelocity impact which created a hole in a panel of the Solar Maximum Mission satellite.

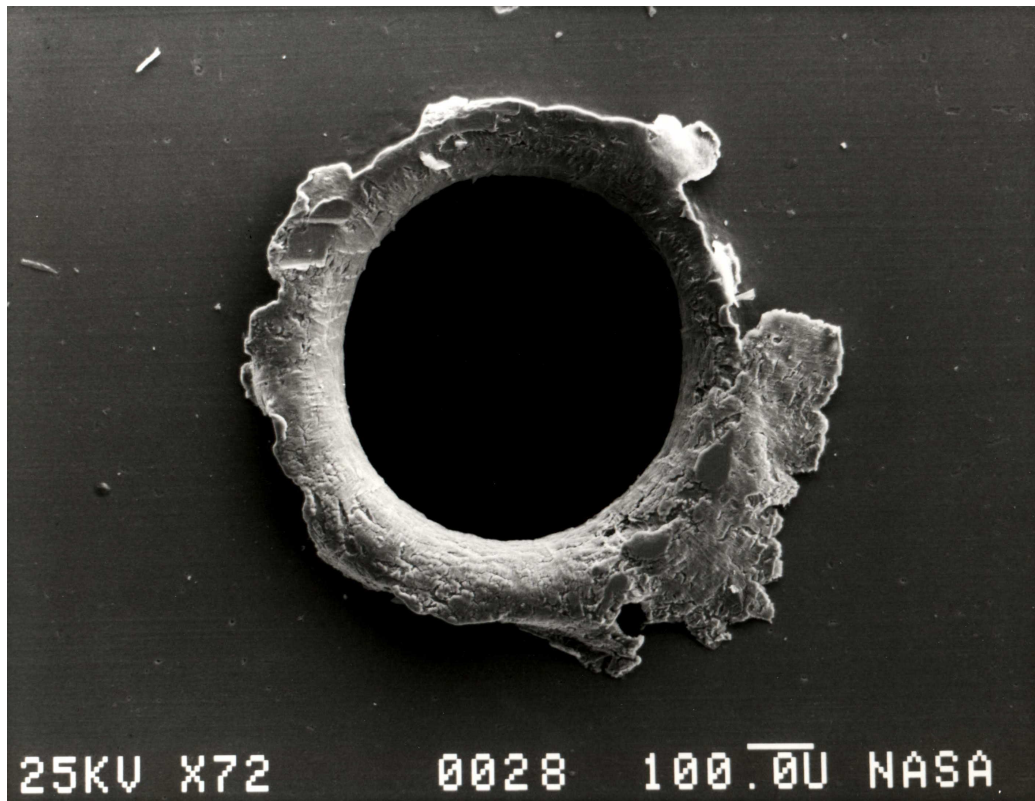


Figure 2.2: A hole made by debris in a solar panel

While delivering payloads into orbit, burning process of solid rocket motors releases particles called SRM slag and SRM dust which are classified as non-fragmentation, unintentional debris and are composed mainly of aluminium oxide. The aim of adding aluminium to most solid fuels is to stabilize the combustion process. SRM slag is fused during the main thrust phase from trapped aluminium oxide, melted aluminium droplets and thermal insulation liner material. Their sizes are between 0.1 and 30 mm. It is assumed that during 1032 SRM firings throughout 44 years, or 2440 up to year 2017 [ESA17], about 1000 tons of propellant were released, 320 of them were aluminium oxide particles (SRM dust) and 4 tons SRM slag. Due to orbital perturbations and different sizes, it is estimated that only 1 ton

CHAPTER 2. INTRODUCTION TO SPACE DEBRIS AND OBSERVATIONS8

of SRM dust and 3 tons of SRM slag remain in the orbit [Kli06]. Figure 2.3 shows a piece of SRM slag recovered from a test firing of a shuttle solid rocket booster.

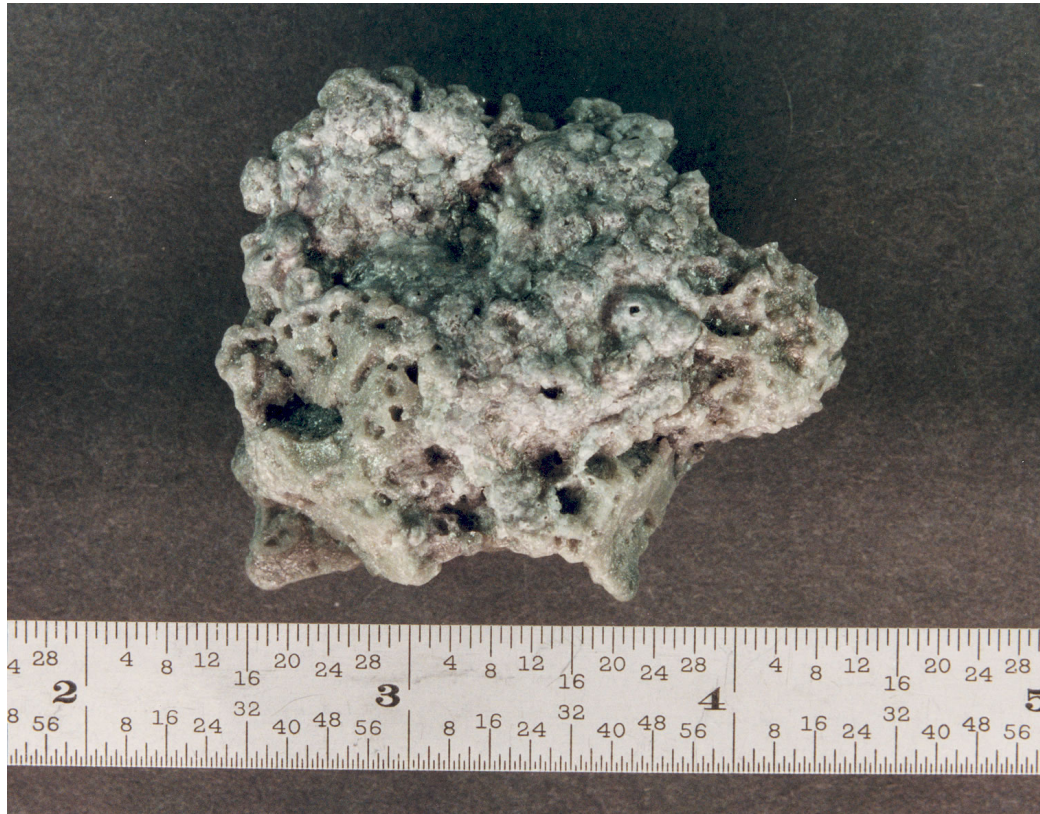


Figure 2.3: SRM slag

Another similar but rare type is droplets of sodium-potassium alloy (NaK), a coolant in Russian RORSAT (Radar Ocean Reconnaissance Satellites). To the contrary to previous methods used to capture and observe small debris, these particles were detected by ground-based radar and optical measurements in the early 1990s. NaK droplets were used in a particular type of reactor used between October 1970 and March 1988, throughout sixteen launch events. It is estimated that whole of 208 kilograms of NaK coolant was released during this period. However, smaller droplets evaporate due to

thermodynamics which puts this type of debris to an estimated mass of 50 to 60 kilograms. Since this kind of reactor is no longer used, NaK droplets along with Westford Needles are considered a historic, non-reproducing space debris.

A communications experiment between years 1961 and 1963 consisted of deploying copper wires around the Earth. These copper wires were 1.78 cm long and $25.4\ \mu\text{m}$ in diameter in the first experiment and $17.8\ \mu\text{m}$ in diameter in the second experiment - see Figure 2.4. They were originally encased in rotating containers and supposed to disperse to form a layer of radio frequency reflecting dipoles. However, the dispersion failed, and the estimated mass of Westford Needles is less than 60 kg in two clusters, first being 40 000 in needles and the second 1000.

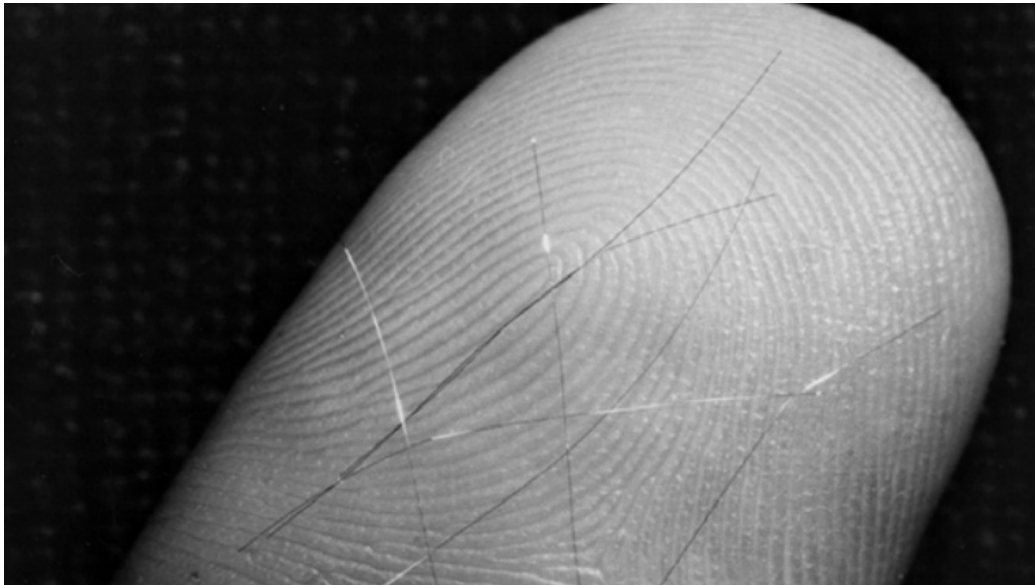


Figure 2.4: Westford needles

While being the major contributor to the population of space debris, small objects are, as mentioned, virtually unobservable from the ground, only by radars and space-based telescopes positioned on LEO, and therefore are not

the main focus of this work.

2.0.2 Large space debris

The most extensive database of tracked objects in orbit is maintained by US Space Surveillance Network (USSSN). As mentioned above, only objects which exceed certain sizes at certain altitudes can be tracked with ground-based radar and optical measurements. Due to this, USSSN incorporates only debris larger than five to ten centimetres in LEO and thirty centimetres to one metre in GEO (geostationary altitudes, approximately 36000 kilometres). Currently, USSSN contains more than 42 thousand tracked objects with more than half of them still in orbit. About 24% of them are satellites and 18% are spent upper stages and other mission-related objects [ESA17]. Out of 175 fragmentation events recorded since 1961 until January 2002, 48 have been categorized as deliberate explosions or collisions, 52 as propulsion system explosions, 10 have been caused by aerodynamic forces, 7 are believed to have been electrical system failures and 1 was an accidental collision [Kli06].

Deliberate collisions have been caused mainly as test scenarios for Strategic Defence Initiative (SDI) experiment. In the first case, an anti-satellite missile was fired and destroyed Solwind P78-1 satellite. The second collision was between the USA-19 spacecraft and an upper stage used to bring it into the orbit. Number of fragments for both of these events was 285 and 13 respectively but as a result of natural cleaning processes or deliberate planning, from H-10 event only 33 objects were on orbit by January 2002 and from Solwind P78-1 only 2. However, the largest fragmentation event occurred in 2007 when China intentionally destroyed its non-functional weather satellite Fengyun-1C, generating more than 3215 new fragments.

Even though unintentional collisions are rare and only 0.2% of all cata-

logged objects until February 2009 have been created in this way it is expected that they will be a major cause for debris in the future. On November 13, 1986 an Ariane-1 H-10 upper stage exploded, causing a fragment cloud containing 488 catalogue entries. The first unintentional in-orbit collision came to pass 10 years later between a French satellite and the mentioned H-10 upper stage explosion fragment. The Cerise satellite was still able to function afterwards and the event caused only one new piece of debris [Ši12].

A particularly interesting class of space debris is anomalous debris. It's a specific group that has small velocity and high area to mass ratio (A/M) and its formation process is unknown. The exemplary member of anomalous debris is multilayer insulation (MLI), and sometimes paint flakes. MLI is used as thermal protection to decrease thermal noise on antennae and satellite buses of spacecrafts. MLI can be divided into two types based on their purpose – as a cover and outer layer, and as a reflector and inner layer.

The rapid creation of new debris of non-negligible sizes is a major concern due to the phenomenon called “Kessler syndrome”. The term was coined in 1978 and it means that “each collision would produce several hundred objects large enough to catalogue, increasing the rate that future collision breakups would occur, resulting in an exponential growth in the collision rate and debris population” (Kessler, 2009).

Spent upper stages and non-functional satellites are one of the largest and most compact space debris. Even though many of them re-enter the Earth's atmosphere on purpose, or are elevated on further orbits and their life on orbit is relatively short, they still pose a threat to functional satellites or missions in progress. Figure 2.5 shows such spent upper stage, specifically Agena D, the most launched American upper stage (Genesis of Agena D, 2006).



Figure 2.5: Agena D upper stage

2.1 Observations and telescopes

Optical telescopes are usually placed at high altitudes, with minimal light pollution and good meteorological and atmospheric conditions. Telescopes used for satellite tracking must be operated at "astronomical night" (Sun being more than 18° under the horizon) while the tracked objects must still be illuminated by the Sun [Kli06].

Telescopes are divided into two groups: refractors and reflectors. The first type uses lens systems to observe objects while the second one uses mirror surfaces to focus incoming light. Reflectors are categorized into four subgroups:

1. Newton telescopes,
2. Cassegrain telescopes,
3. Coudé telescopes,
4. Ritchey-Chrétien telescopes.

The base upon which a telescope is placed is called a mount. As with telescopes, there are many types of mounts with each giving different advantages than the other. Mounts are able to rotate both vertically and horizontally.

A telescope collects photons which are reflected or emitted by a space object. Usually, the origin of photons is the Sun and depending on the angle between the Sun, the object and the observer and reflection efficiency of the target the intensity is determined. The light is then translated into an image which can be viewed by an eyepiece or used to generate an exposure on an Charge-Coupled device (CCD). CCDs are photosensitive and solid-state imaging sensors which convert incoming photons into electric charges

on an array of photodetectors. The time-tagged information coming from the photodetectors can be reconstructed into an image with a resolution depending on the granularity of the CCD. High-end systems use CCD which produce images with resolution of up to 4096 x 8192 pixels. CCDs naturally heat up and the danger of thermal noise corruption is mitigated by using active coolants, such as liquid nitrogen [Kli06].

2.1.1 ESA OGS

European Space Agency (ESA) Optical Ground Station (OGS) is a Zeiss telescope built in the Teide Observatory, in Tenerife, Spain, 2400 m above sea level. It's a one-metre telescope with focal length 13.3 m originally used for tests with laser link, space debris observation and other astronomical night observations. The CCD camera has a field of 4000 x 4000 pixels. The telescope can detect and track near-GEO objects down to 10-15 cm in size and has photometric observations capabilities and therefore can determine material properties of unknown objects and provides information on origin of newly detected fragments. Throughout years 2009 to 2013 the telescope has been credited by Minor Planet Center (MPC) with discovery of 38 minor planets.

Besides being used for mentioned astronomical purposes, its unique location and ability to be tilted to near-horizontal position and point at a different station, namely Jacobus Kapteyn Telescope in La Palma, allows it to be employed in quantum telecommunication experiments. In 2012 a group of researchers funded by ESA successfully transferred physical properties of one particle to another 143 km away via quantum teleportation. The telescope is currently operated by Instituto de Astrofísica de Canarias (IAC).

Figure 2.6 shows the schematic of ESA OGS. One of the most important

parts is the Cassegrain focus where the CCD camera is used for observation of asteroids and for long-term monitoring of comets.

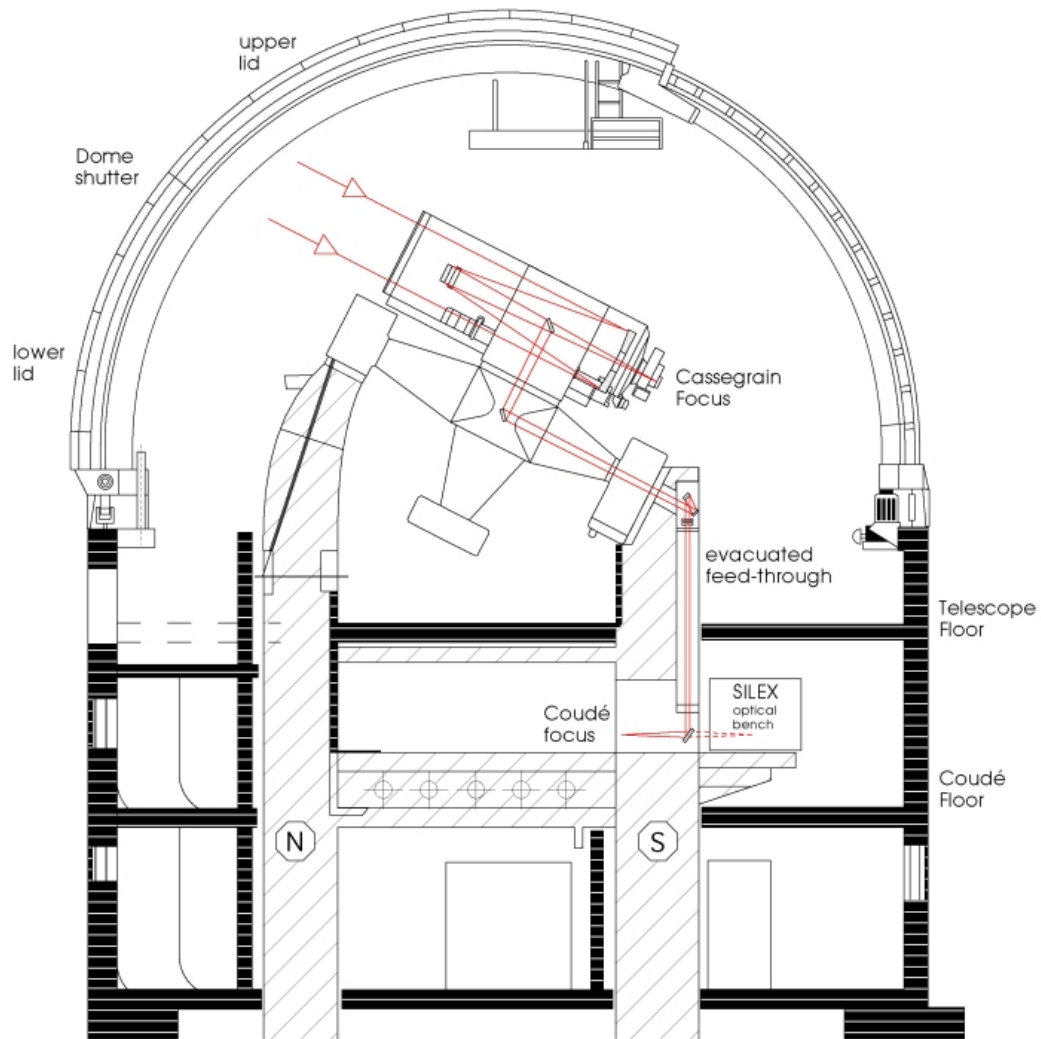


Figure 2.6: ESA OGS schematic

Figure 2.7 is an image of the Zeiss telescope on the English mount.



Figure 2.7: ESA OGS telescope

2.1.2 FMPI AGO

Astronomické a geofyzikálne observatórium (Astronomical and geophysical observatory, or AGO) is located in Modra, Slovakia and belongs to Fakulta matematiky, fyziky a informatiky (Faculty of mathematics, physics and informatics of Comenius University, or FMPI). The observatory has a main reflector telescope with a 0.6m Zeiss telescope with focal length of 3.28m. The CCD camera has resolution of 1024 x 1024 pixels.

Figure 2.8 shows the main telescope which is operated by a computer.



Figure 2.8: The main Zeiss telescope

Chapter 3

Object dynamics

3.1 Kepler's laws of orbital motion

montebruck kniha

3.2 Equatorial coordinate system

montebruck kniha

3.3 CCD and image reference frame

zakladne charakteristiky kamery + x a y (image reference frame)

3.4 Image processing, segmentation and astrometric reduction

mailom

3.5 Initial orbit determination problem

montebruck kniha + phd

Chapter 4

Existing solutions to the problem of tracklet building

4.1 kd-trees

4.1.1 Efficient intra- and inter-night linking of asteroid detections using kd-trees

4.2 Uniform linear motion detection

4.2.1 Optical observation, image-processing, and detection of space debris in GEO

Chapter 5

Technical and practical requirements

5.1 Input data

Information about potential unknown objects are passed to the program in the form of input files. There are two formats of files which contain relevant metadata, such as right ascension, declination, magnitude, and other, which are vital to the correct functioning of algorithms of tracklet building described in detail in chapter 6.

The first is Flexible Image Transport System (FITS), a standardised and the most commonly used digital file format in astronomy. The second is a locally defined format, an output from previous stage of the pipeline, a .cat file.

The formats are described in length in sections 5.1.1 and 5.1.2 respectively.

5.1.1 Flexible Image Transport System files

FITS is the standard archival data format for astronomical data sets.

It was originally designed in year 1981 for transporting image data on magnetic tapes between research institutions. In year 1982, FITS was officially endorsed by International Astronomical Union (IAU) as the format for the interchange of astronomical data. Since then FITS have expanded to accommodate more complex data structures and have evolved from only transporting information into preferred format for archival and analytical purposes.

FITS files in this work are used as a source of data about objects and for image stacking.

File structure

FITS files consist of three main FITS Structures (structures):

- primary header and data unit (HDU, mandatory)
- conforming extensions (optional)
- other special records (optional).

In our case, all FITS Files contain only the primary HDU which is sometimes referred to as Basic FITS File or a Single Image FITS File.

If used, a structure contains a higher than zero number of FITS Blocks (blocks), each with size of 2880 bytes. Primary HDU always starts with the first block and each following structure begins with a block starting right after the end of the last block of previous structure. Furthermore, the primary HDU and each extension HDU must contain non-zero number of 2880-byte FITS Header (header) blocks, which are mandatory, and an optional array

of associated 2880-byte data blocks. There is no explicit limit on the number of blocks and therefore the size of the file.

Data arrays

If not empty, primary data array has size $1x999$ and is represented by continuous stream of bits. Each data value in the array consists of a fixed number of bits which are given in the keyword *BITPIX*. If length of data is shorter than length of final block, the difference is filled by setting the bits to zero. Arrays with more than one dimension are possible but irrelevant in our context.

An example of FITS Data array is shown in Figure

Headers

Headers contain only limited set of text characters encoded in ASCII. Allowed characters are highlighted in Figure 5.1.

Dec	Bin	Hex	Char	Dec	Bin	Hex	Char	Dec	Bin	Hex	Char	Dec	Bin	Hex	Char
0	0000 0000	00	[NUL]	32	0010 0000	20	space	64	0100 0000	40	@	96	0110 0000	60	`
1	0000 0001	01	[SOH]	33	0010 0001	21	!	65	0100 0001	41	A	97	0110 0001	61	a
2	0000 0010	02	[STX]	34	0010 0010	22	"	66	0100 0010	42	B	98	0110 0010	62	b
3	0000 0011	03	[ETX]	35	0010 0011	23	#	67	0100 0011	43	C	99	0110 0011	63	c
4	0000 0100	04	[EOT]	36	0010 0100	24	\$	68	0100 0100	44	D	100	0110 0100	64	d
5	0000 0101	05	[ENQ]	37	0010 0101	25	%	69	0100 0101	45	E	101	0110 0101	65	e
6	0000 0110	06	[ACK]	38	0010 0110	26	&	70	0100 0110	46	F	102	0110 0110	66	f
7	0000 0111	07	[BEL]	39	0010 0111	27	'	71	0100 0111	47	G	103	0110 0111	67	g
8	0000 1000	08	[BS]	40	0010 1000	28	(72	0100 1000	48	H	104	0110 1000	68	h
9	0000 1001	09	[TAB]	41	0010 1001	29)	73	0100 1001	49	I	105	0110 1001	69	i
10	0000 1010	0A	[LF]	42	0010 1010	2A	*	74	0100 1010	4A	J	106	0110 1010	6A	j
11	0000 1011	0B	[VT]	43	0010 1011	2B	+	75	0100 1011	4B	K	107	0110 1011	6B	k
12	0000 1100	0C	[FF]	44	0010 1100	2C	,	76	0100 1100	4C	L	108	0110 1100	6C	l
13	0000 1101	0D	[CR]	45	0010 1101	2D	-	77	0100 1101	4D	M	109	0110 1101	6D	m
14	0000 1110	0E	[SO]	46	0010 1110	2E	.	78	0100 1110	4E	N	110	0110 1110	6E	n
15	0000 1111	0F	[SI]	47	0010 1111	2F	/	79	0100 1111	4F	O	111	0110 1111	6F	o
16	0001 0000	10	[DLE]	48	0011 0000	30	0	80	0101 0000	50	P	112	0111 0000	70	p
17	0001 0001	11	[DC1]	49	0011 0001	31	1	81	0101 0001	51	Q	113	0111 0001	71	q
18	0001 0010	12	[DC2]	50	0011 0010	32	2	82	0101 0010	52	R	114	0111 0010	72	r
19	0001 0011	13	[DC3]	51	0011 0011	33	3	83	0101 0011	53	S	115	0111 0011	73	s
20	0001 0100	14	[DC4]	52	0011 0100	34	4	84	0101 0100	54	T	116	0111 0100	74	t
21	0001 0101	15	[NAK]	53	0011 0101	35	5	85	0101 0101	55	U	117	0111 0101	75	u
22	0001 0110	16	[SYN]	54	0011 0110	36	6	86	0101 0110	56	V	118	0111 0110	76	v
23	0001 0111	17	[ETB]	55	0011 0111	37	7	87	0101 0111	57	W	119	0111 0111	77	w
24	0001 1000	18	[CAN]	56	0011 1000	38	8	88	0101 1000	58	X	120	0111 1000	78	x
25	0001 1001	19	[EM]	57	0011 1001	39	9	89	0101 1001	59	Y	121	0111 1001	79	y
26	0001 1010	1A	[SUB]	58	0011 1010	3A	:	90	0101 1010	5A	Z	122	0111 1010	7A	z
27	0001 1011	1B	[ESC]	59	0011 1011	3B	;	91	0101 1011	5B	[123	0111 1011	7B	{
28	0001 1100	1C	[FS]	60	0011 1100	3C	<	92	0101 1100	5C	\	124	0111 1100	7C	
29	0001 1101	1D	[GS]	61	0011 1101	3D	=	93	0101 1101	5D]	125	0111 1101	7D	}
30	0001 1110	1E	[RS]	62	0011 1110	3E	>	94	0101 1110	5E	^	126	0111 1110	7E	~
31	0001 1111	1F	[US]	63	0011 1111	3F	?	95	0101 1111	5F	_	127	0111 1111	7F	[DEL]

Figure 5.1: Allowed ASCII characters

A header contains at least one header block, each consisting of maximum 80-character keyword sequence. In the 2880-byte block, this puts the number of records at 36. The logical end of the block is marked by the END keyword and if there is space left, it is filled with ASCII space.

Keywords are composed of key-value pairs and an optional comment. The presence of the value indicator ('= ', ASCII symbol "equals" followed by ASCII space) determines that the key has a value associated with it. The values field can hold any of the following types:

- character string (eg. '27/10/82')
- logical value (represented as *T* or *F*)
- integer number (eg. 12)
- real floating-point number (eg. -12.5)
- complex integer number (eg. $2 + 4i$)
- complex floating-point number (eg. $7.8 + 1.7i$).

Each FITS file must contain several mandatory keywords (such as *SIMPLE* - describes whether FITS file is a Basic Fits File or not; *END* - marks logical end of a block) which are reserved and have fixed types of their values. FITS format also contains reserved keywords that are not mandatory (such as *DATE* - date on which the HDU was created; other).

In our case, the most relevant keywords are *DATE-OBS* and *EXPTIME*, or *EXPOSURE* in files where the keyword *EXPTIME* is missing.

An example of FITS Header is shown in Figure 5.2.

Header	IMAGE
SIMPLE =	T
BITPIX =	16 /8 unsigned int, 16 & 32 int, -32 & -64 real
NAXIS =	2 /number of axes
NAXIS1 =	1024 /fastest changing axis
NAXIS2 =	1024 /next to fastest changing axis
BSCALE =	1.0000000000000000 /physical = BZERO + BSCALE*array_value
BZERO =	32768.000000000000 /physical = BZERO + BSCALE*array_value
OBJECT =	' '
TELESCOP=	' /' telescope used to acquire this image
INSTRUME=	'FLI' /' instrument or camera used
OBSERVER=	' '
NOTES =	' '
DATE-OBS=	'2017-09-22T18:59:07' /YYYY-MM-DDThh:mm:ss observation start, UT
EXPTIME =	7.0000000000000000 /Exposure time in seconds
EXPOSURE=	7.0000000000000000 /Exposure time in seconds
SET-TEMP=	-40.0000000000000000 /CCD temperature setpoint in C
CCD-TEMP=	-40.0000000000000000 /CCD temperature at start of exposure in C
XPIXSZ =	24.0000000000000000 /Pixel Width in microns (after binning)
YPIXSZ =	24.0000000000000000 /Pixel Height in microns (after binning)
XBINNING=	1 /Binning factor in width
YBINNING=	1 /Binning factor in height
XORGSUB=	0 /Subframe X position in binned pixels
YORGSUB=	0 /Subframe Y position in binned pixels
IMAGETYP=	'Light Frame' /' Type of image
FOCALLEN=	0.0000000000000000 /Focal length of telescope in mm
APTDIA =	0.0000000000000000 /Aperture diameter of telescope in mm
APTAREA =	0.0000000000000000 /Aperture area of telescope in mm^2
SWCREATE=	'MaxIm DL Version 5.02' /Name of software that created the image
SBSTDVER=	'SBFITSEXT Version 1.0' /Version of SBFITSEXT standard in effect
FLIPSTAT=	' '
SWOWNER =	'Harvester' /' Licensed owner of software
RA =	'20:32:55.72' /Image center Ra, solved by Astrometry.net
DEC =	'+7:41:13.0' /Image center Dec, solved by Astrometry.net

Figure 5.2: FITS Header example

5.1.2 .cat files

.cat files are text files generated by the Astrometrica tool. Astrometrica tool accepts FITS files (see 5.1.1) as input, provides interactive graphical user interface to manipulate each FITS file and performs Astrometrical reduction resulting in an output file with the extension .cat. Detailed description of the contents of a .cat file is in the following subsection.

Contents of a .cat file

First four lines of a .cat file are header - first line is empty, second is name of the colum, third contains units in which are values in specific column represented and fourth is a separator (see Figure 5.3).

Type	RA	dRA	Dec.	dDec	R	dR	x	y	Flux	FWHM	Peak	Fit	Designation
	h m s	"	° ' "	"	mag	mag			ADU	"	SNR	RMS	

Figure 5.3: .cat header columns

Meaning of each column is as follows:

1. Type - column outlining the type of a detected object; has four valid values
 - R - a star which has been matched with the star catalogue; if the value is in parentheses, the deviation between the two is too large
 - H - a manually marked object
 - S - a star which has not been matched with the star catalogue
 - ? - an unknown object
2. RA - right ascension in hours/minutes/seconds (see Chapter 3, Section 3.2)
3. dRA - deviation of values of RA between centroid created by Astrometrica and the star catalogue
4. Dec. - declination in degrees/minutes/seconds (see Chapter 3, Section 3.2)
5. dDec - deviation of values of DEC between centroid created by Astrometrica and the star catalogue
6. R - brightness in magnitude
7. dR - deviation of values of brightness between centroid created by Astrometrica and the star catalogue

8. x - position of an object in FITS file on x axis
9. y - position of an object in FITS file on y axis
10. Flux - total intensity of all pixels in ADU (analog to digital unit)
11. FWHM - "*full width at half maximum*" describes a measurement of the width of a diffused object
12. Peak - signal to noise ration - describes the difference between the pixel with maximal value and background
13. Fit - the deviation of fitting of centroids in image to the star catalogue
14. Designation - an user given input

5.1.3 Processing server parameters

The server is a high CPU computer with Linux operating system capable of remote access for multiple users via console or x2goclient. The server is a Supermicro SuperServer 7048R-TR with an Intel® Xeon® E5-2640 v4 with Intel® Turbo Boost Technology, hyper-threading and virtualization capabilities. It also contains 32GB of ECC DDR4 SDRAM 72-bit system memory, 400GB SSD system disk and 4TB SATA 3.0 HDD in RAID1 configuration for additional data storage. 920W power supply and free slots for an additional CPU, system memory sticks and GPUs provide for possible upgrade in the future.

Chapter 6

Proposed solutions

6.1 Use of linear regression

6.2 Use of neural network

6.3 Use of the Initial Orbit Determination algorithms

6.4 Use of Hough transform

Chapter 7

Design and implementation

Chapter 8

Results

8.1 TDM, MPC, and CCSDS data formats

8.2 Visualization of results

8.3 Parameters

Chapter 9

Conclusion

Bibliography

- [ESA17] ESA. Space debris: the esa approach. Brochure, 2017.
- [Kli06] H. Klinkrad. *Space Debris: Models and Risk Analysis*. Astronautical Engineering. Springer, 2006.
- [otPUoOSSS99] United Nations. General Assembly. Committee on the Peaceful Uses of Outer Space. Scientific and Technical Subcommittee. *Technical report on space debris: text of the report adopted by the Scientific and Technical Subcommittee of the United Nations Committee on the Peaceful uses of Outer Space*. United Nations, 1999.
- [Ši12] Jiří Šilha. *Identification of the Artifical Objects in Close Vicinity of the Earth*. PhD thesis, Comenius University, 2012.